https://doi.org/10.5194/acp-2020-176
Preprint. Discussion started: 28 April 2020

Atmospheric Chemistry and Physics Discussions

Characterization and source apportionment of aerosol light scattering in a typical polluted city in Yangtze River Delta, China

Dong Chen[1, 2], Yu Zhao[1, 3*], Jie Zhang[2, 3], Huan Yu[4], Xingna Yu[4]

1. State Key Laboratory of Pollution Control & Resource Reuse and School of the Environment, Nanjing University, 163 Xianlin Ave., Nanjing, Jiangsu 210023, China

2. Jiangsu Provincial Academy of Environmental Science, 176 North Jiangdong Rd., Nanjing, Jiangsu 210036, China

3. Collaborative Innovation Center of Atmospheric Environment and Equipment Technology, CICAEET, Nanjing, Jiangsu 210044, China

4. School of Environmental Science and Engineering, Nanjing University of Information Science and Technology, Nanjing, Jiangsu 210044, China

*Corresponding author: Yu Zhao

Phone: 86-25-89680650; email: yuzhao@nju.edu.cn

https://doi.org/10.5194/acp-2020-176
Preprint. Discussion started: 28 April 2020

Atmospheric Chemistry and Physics Discussions

ABSTRACT

Through online observation and offline chemistry analysis of samples at suburban, urban and industrial sites (NJU, PAES and NUIST respectively) in Nanjing, a typical polluted city in Yangtze River Delta, we optimized the aerosol light scattering estimation method, identified its influencing factors, and quantified the contributions of emission sources to aerosol scattering. The daily average concentration of $PM_{2.5}$ during the sampling period (November 2015-March 2017) was 163.1 ± 13.6 μg/m^3 for the heavily polluted period, 3.8 and 1.6 times those for the clean (47.9 ± 15.8 μg/m^3) and lightly polluted (102.1 ± 16.4 μg/m^3) periods, respectively. The largest increase in PM concentration and its major chemical components was found at the size range of 0.56-1.0 μm for the heavily polluted period, and the contributions of nitrate and sulfate were the greatest in the 0.56-1.0 μm fraction (19.4-39.7% and 18.1-34.7% respectively) for all the three periods. The results indicated that the large growth of nitrate and sulfate were one of the major reasons for the polluted periods. Based on measurements at the three sites, the US IMPROVE algorithm was optimized to evaluate aerosol scattering in eastern China. The light-absorption capacity OC was estimated to account for over half of the methanol soluble organic carbon (MSOC) at NJU and PAES, whereas the fraction was lower at NUIST. Based on Mie theory, we found that the high relative humidity (RH) could largely enhance the light scattering effect of accumulation particles, but it had few effects on the mixing state of particles. The scattering coefficients of particles within the 0.56-1.0 μm range contributed the most to the total scattering (28-69%). The mass scattering efficiency (MSE) of sulfate and nitrate increased with the elevated pollution level, whereas a low MSE of organic matter (OM) was found for the heavily polluted period, probably because a proportion of OM had only light-absorption property. A coupled model of positive matrix factorization (PMF) and Mie theory was developed and applied for the source apportionment of aerosol light scattering. Coal burning, industry and vehicles were identified as the major sources of the reduced visibility in Nanjing, with an estimated collective contribution at 64-70%.

https://doi.org/10.5194/acp-2020-176
Preprint. Discussion started: 28 April 2020


Atmospheric Chemistry and Physics Discussions

The comparison between the clean and polluted period suggested that the increased primary particle emissions from vehicles and industry were the major causes of the visibility degradation in urban and industrial regions, respectively. In addition, secondary aerosols were a great contributor to the reduced visibility.

1 INTRODUCTION

Atmospheric aerosols play a great role in visibility degradation, radiative balance variation and climate (Liu et al., 2017; Malm and Hand, 2007; Zhang et al., 2017), resulting largely from their light extinction (Seinfeld and Pandis, 2006). Understanding the contributions of individual chemical species to aerosol light extinction is important for policy making to alleviate the reduced visibility in cities with aerosol pollution. Studies have estimated that the aerosol single scattering albedo (the fraction of light scattering coefficient to the total extinction) ranges from 0.81-0.93 in urban China (Andreae et al., 2008; Cao et al., 2012; Xu et al., 2002; Xu et al., 2012), implying that the deteriorated visibility primarily results from the scattering effect of aerosols.

Aerosol light scattering is greatly affected by its chemical composition and hygroscopic growth (Liu et al., 2008; Tao et al., 2014a). Based on estimation of the mass scattering efficiency (MSE) of different chemical components, previous studies found that nitrate, sulfate, sea salt and organic matter (OM) are the dominant contributors to aerosol scattering. Developed based on the long-term observations in national parks, the US “IMPROVE” (Interagency Monitoring of Protected Visual Environments) algorithm has been applied to calculate the light extinction of chemical species in aerosols (Watson et al., 2002). Two versions of IMPROVE algorithms (IMPROVE1999 and IMPROVE2007 hereinafter) were deduced successively (Lowenthal and Naresh, 2003; Pitchford et al., 2007), and both assumed that OM has no light-absorption capacity and only light-scattering capacity. As part of OM, however, brown carbon (BrC) has been highlighted in recent studies for its light absorption in the near UV region (Alexander et al., 2008; Bond et al., 2006; Ramanathan et al., 2007; Zhang et al., 2017), and consideration of the light-absorption

https://doi.org/10.5194/acp-2020-176
Preprint. Discussion started: 28 April 2020


Atmospheric Chemistry and Physics Discussions

effect of OM in the optimization process of the IMPROVE formula could improve the understanding of aerosol optical capacity by chemical species (Yan et al., 2014). In addition, hygroscopic growth is a key factor influencing aerosol light scattering (Schwartz, 1996). Previous studies have shown that the light scattering of sulfate and nitrate in $PM_{2.5}$ could be largely enhanced at high relative humidity (RH) conditions (Titos et al., 2016). Aerosol hygroscopicity is expected to depend largely on the particle size and the abundance of water-soluble chemical components (Swietlicki et al., 2008; Tang, 1996). Through the theoretical calculation, Liu et al. (2014) found that smaller particles were in highly hygroscopic mode, whereas larger particles were in nearly hydrophobic mode.

Recently, many studies have been conducted on the relationships between visibility and aerosol light scattering in China (Cheng et al., 2015; Tao et al., 2014b; 2014c; Xue et al., 2010; Zhang et al., 2015). They found the abundance of hygroscopic NH_4NO_3 and $(NH_4)_2SO_4$ in $PM_{2.5}$ and their characteristics were the important reason visibility reduction. However, few studies have analyzed the size distribution of aerosol light scattering or quantified the contributions of different emission source categories to the aerosol light scattering, particularly at the varied air pollution levels. The roles of particles of different sizes and origins on visibility degradation remained unclear. To fill this knowledge gap, this study conducted campaigns at three multiple-functional sites in Nanjing, a mega city located in eastern China. Nanjing suffered relatively heavy aerosol pollution in the Yangtze River Delta (YRD) attrited to the massive emissions of anthropogenic air pollutants (Zhao et al., 2015). The mixed sources of primary aerosols (e.g., coal burning) and secondary aerosol precursors (e.g., vehicle and petrochemical industry) make Nanjing a typical city to study the multiple influential factors of aerosol light scattering (Chen et al., 2019). Combining online and offline techniques at different functional regions, the IMPROVE algorithm was optimized taking the light-absorption OM into account. The influences of aerosol size distributions and pollution levels on the aerosol scattering effect were quantitatively evaluated based on comprehensive analysis of the chemical compositions of particles by size and location. To explore the reasons for the

https://doi.org/10.5194/acp-2020-176
Preprint. Discussion started: 28 April 2020


Atmospheric Chemistry and Physics Discussions

visibility reduction in different functional regions, a new coupled PMF-Mie model was developed and the source apportionments of aerosol light scattering were determined for the clean and polluted periods.

2 METHODOLOGY

2.1 Site description

The campaigns were conducted at three sites in Nanjing, i.e., NJU, PAES and NUIST, representative for the suburban, urban and industrial region, respectively (see the site locations in Figure S1 in the Supplement). NJU (32.07°N, 118.57°E) was on the roof (25 m above the ground) of the School of the Environment building in the Nanjing University campus in eastern suburban Nanjing (Chen et al., 2017; 2019). PAES (32.03°N, 118.44°E) was on the roof (30 m above the ground) of the Jiangsu Provincial Academy of Environmental Science building in western urban Nanjing. The site was surrounded by heavy traffic and commercial and residential buildings (Li et al., 2015). NUIST (32.21°N, 118.72°E) was on the roof of the School of the Environment building in the Nanjing University of Information Science & Technology campus. It was an industrial pollution site influenced by the nearby power, iron & steel, and petrochemical industry plants (Wang et al., 2016a).

2.2 Aerosol sampling and chemical analysis

Pre-combusted (at 500 °C for ~5 h) quartz filters (90 mm in diameter, Whatman International Ltd., UK) were applied for $PM_{2.5}$ sampling. The filter samples were weighed before and after sampling under the constant temperature (23±2°C) and RH (40±3%) for 24 hours conditioning. All the $PM_{2.5}$ samples were collected using the TH-150C sampler (Wuhan Tianhong Ltd., China) at a flow rate of 100 L/min. From November 2015 to March 2017, 282 daily $PM_{2.5}$ samples at the three sites (174 for NJU, 45 for PAES and 63 for NUIST) were collected.

Three sets of ten-stage Micro-Orifice Uniform Deposit Impactors (MOUDI, Model 110, MSP Corp., USA) were adopted to collect size-segregated particles. The 50% cutoff points of the MOUDI-110 were 18, 10, 5.6, 3.2, 1.8, 1.0, 0.56, 0.32, 0.18

https://doi.org/10.5194/acp-2020-176
Preprint. Discussion started: 28 April 2020


Atmospheric Chemistry and Physics Discussions

and 0.056 μm. Loaded with Teflon and quartz filters (47 mm in diameter, Whatman International Ltd., UK), MOUDI was operated at a flow rate of 30 L/min. To obtain sufficient particles at each stage for the chemical analysis, every sampling lasted continuously for 24 h from 9:00am. Seventy-five sets of particle samples were obtained from December 2015 to February 2017 at NJU, 25 sets were obtained from August 2016 to January 2017 at PAES, and 31 sets were obtained from July 2016 to February 2017 at NUIST.

Three anions (SO_4^{2-}, NO_3^- and Cl^-) and five cations (Na^+, NH_4^+, K^+, Mg^{2+}, and Ca^{2+}) in particles were measured in the extracted solution of the filter samples with ion chromatography (Dx-120, Dionex Ltd., USA). CS12A column (Dionex Ltd.) with 20 mM MSA eluent and AS11-HC column (Dionex Corp.) with 8 mM KOH eluent were used to measured cations and anions, respectively (Chen et al., 2019). Elemental carbon (EC) and organic carbon (OC) were measured with an OC-EC aerosol analyzer (Sunset Inc., USA) following the thermal-optical transmittance (TOT) protocol. More details on the analyzer operation were described in our previous studies (Chen et al., 2017; 2019). Recent studies indicated that methanol soluble organic carbon (MSOC) was a more suitable BrC surrogate than water soluble organic carbon (WSOC) and was thus used in present study (Cheng et al., 2016; 2017; Huang et al., 2018; Lei et al., 2018). The analytical procedure was described in details in Chen et al. (2019). Elements of size-resolved particles collected in the Teflon filters (As, Al, Ba, Cd, Co, Cr, Cu, Fe, Mn, Mo, Ni, Ti, V, and Zn) were measured with an inductively coupled plasma-mass spectrometer (ICP-MS, PerkinElmer ELAN 9000, USA) in order to provide further information on the aerosol sources. More detailed information on the instrument was provided by Khan et al. (2016) including the precision, calibration, detection limit, and analytical procedures.

2.3 Measurements of real time aerosol scattering coefficients

The aerosol scattering coefficients were measured using two different types of integrating nephelometers, i.e., Aurora 1000G (Ecotech Pty Ltd., Australia) at NJU and PAES, and Model 3563 (TSI Inc., USA) at NUIST. To obtain the dry aerosol

https://doi.org/10.5194/acp-2020-176
Preprint. Discussion started: 28 April 2020


Atmospheric Chemistry and Physics Discussions

scattering coefficient, the three nephelometers controlled the RH of the inflow air under 50% by the heated inlet to mitigate the impact of water vapor on the scattering coefficient. The nephelometers at NJU and PAES were operated at a flow rate of 5 L/min, and that at NUIST was at 20 L/min. Routine maintenance including zero calibration and span check was conducted following the instrument manual.

To explore the RH impact on aerosol light scattering, an online monitoring instrument Cavity Attenuated Phase Shift Albedo monitor (CAPS, Shoreline Science Research Inc., Japan) was used to measure the ambient scattering coefficient at NJU in real ambient conditions. The instrument operates at the wavelength of 530 nm (Onasch et al., 2015; Petzold et al., 2013), and more details on its operation during the campaigns were provided by Chen et al. (2019).

2.4 Data analysis

2.4.1 Estimation of the scattering coefficient of aerosol chemical species with different methods

The details of IMPROVE1999 and IMPROVE2007 are summarized in the Supplement Section A1. Neglecting the light-absorbing effect of BrC, the two algorithms could overestimate the scattering coefficient of OM (Yan et al., 2014). The major difference between the two versions is that the IMPROVE2007 algorithm considers the variety of mass scattering efficiencies due to particle size for $(NH_4)_2SO_4$, NH_4NO_3 and OM. In this study, multiple linear regressions between the measured light scattering components and aerosol scattering coefficients were conducted to obtain the mass scattering efficiency (MSE) considering the presence of BrC. The measured scattering coefficients were subtracted from the scattering coefficients of sea salt, soil dust and coarse particles. The $PM_{2.5}$ scattering coefficient can be estimated statistically based on the concentrations of individual chemical species as Eq. (1):

https://doi.org/10.5194/acp-2020-176
Preprint. Discussion started: 28 April 2020

Atmospheric Chemistry and Physics Discussions

$$
\begin{aligned}
b_{sca} = {} & a \times f_S(RH)[Small\ (NH_4)_2SO_4] + b \times f_L(RH)[Large\ (NH_4)_2SO_4] \\
& + c \times f_S(RH)[Small\ NH_4NO_3] + d \times f_L(RH)[Large\ NH_4NO_3] \\
& + e \times \left([Small\ OM] - m \times [Small\ MSOC]\right) \\
& + f \times \left([Large\ OM] - n \times [Large\ MSOC]\right)
\end{aligned} \tag{1}
$$

where b_{sca} is the measured $PM_{2.5}$ scattering coefficient; a, c and e are the MSEs of $(NH_4)_2SO_4$, NH_4NO_3 and OM (except for light-absorbing BrC) in the small size mode, respectively; b, d and f are the MSEs of $(NH_4)_2SO_4$, NH_4NO_3 and OM (except for light-absorbing BrC) in the large size mode, respectively (definitions of small and large size modes for various aerosol components can be referred to Malm et al. (2007)); m and n indicate the mass fractions of light-absorbing BrC to total MSOC in small and large modes, respectively; $f(RH)$ (including $f_L(RH)$ and $f_S(RH)$) of sulfate and nitrate indicate the scattering hygroscopic growth factor under a given relative humidity (RH), obtained from Pitchford et al. (2007).

In addition to $PM_{2.5}$, the scattering coefficient for particles at a given size ($b_{sca}(RH)$) is calculated with the Mie theory (Bohren et al., 1998; Cheng et al., 2015):

$$
b_{sca}(RH) = \int \pi [D_p \times \frac{g(RH)}{2}]^2 \times Q_{sca}[m(RH),\ Dp,\ \lambda] \times N(D_p) \times g(RH) dD_p \tag{2}
$$

where $m(RH)$ is the aerosol refractive index; $g(RH)$ is the hygroscopic growth factor; Q_{sca} is the scattering efficiency for a single spherical particle with diameter D_p and can be calculated with the Mie theory by inputting D_p, $m(RH)$ and the incident wavelength (λ); $N(D_p)$ is the number concentration of particle with diameter D_p. In general, three typical models are proposed to represent the particle mixing state including internal, external and core-shell mixture (Jacobson, 2001; Seinfeld and Pandis, 2006). The methods of calculating the parameters including $m(RH)$ and $N(D_p)$ are different for the three mixed states, and the details can be referred to Ding et al. (2015).

2.4.2 Source apportionment of aerosol scattering coefficients with a coupled model of PMF and Mie theory

Positive matrix factorization (PMF) is an effective technical method for source apportionment of atmospheric aerosols (Kim and Hopke, 2004). In this study, PMF 5.0 software was applied in the source apportionment of accumulated mode particles.

https://doi.org/10.5194/acp-2020-176
Preprint. Discussion started: 28 April 2020


Atmospheric Chemistry and Physics Discussions

In total, 245, 145 and 163 aerosol samples were analyzed at NJU, PAES and NUIST, respectively. It is currently difficult to resolve the sources of secondary organic aerosol (SOA) with PMF. In this study, a simplified method was applied to differentiate the sources of primary and secondary aerosols. Organic carbon is split into primary and secondary organic carbon (POC and SOC), and the SOC concentration was calculated with the EC-tracer method (Chen et al., 2017). The source contributions of primary particles were obtained using the PMF model, and those of secondary inorganic aerosol (SIA) and SOA were further determined based on estimates of the nitrogen oxides (NO_x), sulfur dioxide (SO_2) and volatile organic compounds (VOCs) emissions in a local inventory (Huang, 2018; Lang et al., 2017; Wang et al., 2015). The chemical components applied in the PMF model included inorganic ions, carbonaceous components and metallic elements. We followed the method described in the PMF manual and Tian et al. (2016) to calculate the chemical component uncertainties in the measurement dataset. Criteria including the optimum number of factors and the minimization of an objective function Q were determined based on the principles described in previous studies (Moon et al., 2008; Tian et al., 2016; Watson et al., 2015) and applied in the model to obtain the best PMF solution.

A coupled model combining PMF and the Mie theory was developed to evaluate the sources of aerosol light scattering. The procedure of the method was as follows: (1) the EPA-PMF model was applied to quantify the contributions of different sources to the mass concentrations of chemical species in size-segregated particles; (2) the contribution (%) of the i^{th} chemical component to the aerosol scattering coefficient at size D_p was estimated based on Mie theory; (3) the percentage contribution (%) of the i^{th} component in the j^{th} source category to the total scattering at size D_p was calculated as the product of the percentage contribution (%) of the i^{th} chemical species to the total scattering and that of the j^{th} source category to the mass concentration of the i^{th} species in the particles at size D_p, as indicated in Eq.(3); and (4) the percentage contribution (%) of the j^{th} source to the total scattering at size D_p was estimated by summing η_{ijDp}, as shown in Eq. (4).

https://doi.org/10.5194/acp-2020-176
Preprint. Discussion started: 28 April 2020

Atmospheric Chemistry and Physics Discussions

$$\eta_{ijDp} = a_{ijDp} \frac{b_{iDp}}{\sum_{i=1}^{m} b_{iDp}} \times 100\% \quad (3)$$

$$\eta_{jD_p} = \sum_{i=1}^{I} \eta_{ijD_p} \quad (4)$$

where i and j stand for the numbers of aerosol chemical components and potential sources, respectively; η_{ijDp} (%) is the contribution (%) of i^{th} scattering component in the j^{th} source to the total particle scattering at size D_p; η_j (%) is the contribution (%) of the j^{th} source to the total scattering at size D_p; a_{ijDp} is the relative contribution (%) of the j^{th} source to the i^{th} chemical component in particles with size D_p from PMF modeling; and b_{iDp} is the contribution of the i^{th} chemical component to the total scattering from Mie modeling.

3 RESULTS AND DISCUSSION

3.1 Mass concentrations and size distributions of PM compositions

Based on the national definition on ambient Air Quality Index (AQI) (MEP, 2012), we divided the whole sampling period into three categories, i.e., the clean period with AQI less than 100, the lightly polluted period with AQI between 100 and 200, and the heavily polluted period with AQI above 200. Note that the AQI is a unitless index calculated based on the daily concentrations of regulated air pollutants including NO_2, SO_2, CO, O_3, $PM_{2.5}$ and PM_{10} (MEP, 2012). As summarized in Table 1, the average daily $PM_{2.5}$ mass concentrations at the three conditions were calculated at 47.9 ± 15.8, 102.1 ± 16.4, and 163.1 ± 13.6 μg/m^3, respectively. The mass concentration of secondary inorganic ions (SO_4^{2-}, NO_3^- and NH_4^+) for the heavily polluted period was 4.4 and 2.2 times those for the clean and lightly polluted periods, respectively. The corresponding values for the carbonaceous aerosols (the sum of OC and EC) were 3.1 and 1.9 times, respectively, and the OC to EC ratios increased from 4.5 for the clean period to 5.2 for the heavy period. In addition to the particulate components, gaseous pollutants such as NO_2 and SO_2 were also significantly elevated from the clean to the heavy periods. These results imply that secondary aerosol

https://doi.org/10.5194/acp-2020-176
Preprint. Discussion started: 28 April 2020


Atmospheric Chemistry and Physics Discussions

formation was an important source of enhanced $PM_{2.5}$ for the heavily polluted period.

Figure S2 in the Supplement compares the size distributions of mass concentrations for particles and selected chemical components under three pollution levels. Bimodal size distributions were found for PM and OC mass concentrations, with the two peaks at the ranges of 0.56-1.0 μm and 3.2-5.6 μm, respectively. This bimodal pattern could partly result from the coexistence of primary and secondary sources of OC. POC with larger sizes may contribute largely to the peak in the coarser particles. In contrast, due to chemistry reactions of biogenic and anthropogenic VOCs, SOC was expected to be abundant in the accumulation mode (0.18-1.8 μm) (Cao et al., 2007). The size distributions of NO_3^- and SO_4^{2-} followed a unimodal distribution with the mass concentrations peak at the range of 0.56-1.0 μm, as most of the inorganic aerosols were generated through secondary formation. The mass concentrations of PM, NO_3^-, SO_4^{2-} and OC for all sizes were enhanced from the clean to the polluted periods, and the biggest differences were found in the size bin of 0.56-1.0 μm. As shown in Figure S2a, the concentrations of $PM_{0.56-1.0}$ for the heavily and lightly pollution periods were 7.0 and 2.7 times greater than that for the clean period, respectively. Moreover, $PM_{0.56-1.0}$ contributed 31%, 23%, and 15% to the total mass concentrations of particles for the heavily, lightly polluted and clean periods, respectively, implying that the enhanced concentration of $PM_{0.56-1.0}$ was an important reason for the aggravated pollution. As shown in Figure S2b-S2d, the sum of NO_3^-, SO_4^{2-} and OC for the heavily polluted period was 10.7 and 2.9 times greater than those for the lightly polluted and clean periods, respectively. From clean to heavily polluted periods, the collective mass fraction of the three components to $PM_{0.56-1.0}$ increased from 42% to 64%. The results indicated that the increased NO_3^-, SO_4^{2-} and OC at the size bin of 0.56-1.0 μm could be an indicator for the serious air pollution events.

To explore the mass fractions of major chemical species in the particles, the PM mass was reconstructed as $(NH_4)_2SO_4$ ($1.38\times SO_4^{2-}$), NH_4NO_3 ($1.29\times NO_3^-$), OM ($1.55\times$OC), fine soil (FS) and EC (Cheng et al., 2015; Pitchford et al., 2007). As shown in Figure S3 in the Supplement, strong correlations were found between the reconstructed PM mass concentrations and the measurements for $PM_{1.8}$ (R^2=0.85) and

https://doi.org/10.5194/acp-2020-176
Preprint. Discussion started: 28 April 2020


Atmospheric Chemistry and Physics Discussions

302 PM_{10} (R^2=0.81) at the three sites. The slope of $PM_{1.8}$ (0.80) was greater than that of
303 PM_{10} (0.65), indicating smaller unidentified fraction in the $PM_{1.8}$. The larger
304 unidentified mass in the reconstructed PM_{10} was probably due to underestimation in
305 the crustal components (Hueglin et al., 2005).

306 Figure 1 presents the mass concentrations and fractions of the reconstructed
307 aerosol chemical species by particle size under the three pollution levels. NH_4NO_3,
308 $(NH_4)_2SO_4$, and OM were the dominant components in particles. From the clean to
309 heavily polluted periods, their mass fractions to $PM_{1.8}$ increased from 16.9 to 35.3%,
310 from 14.9 to 28.6% and from 16.7 to 22.2%, respectively (Figure 1b, Figure 1d and
311 Figure 1f). The mass fraction of OM in $PM_{1.8}$ was 5.4% and 7.4% larger than
312 NH_4NO_3 and $(NH_4)_2SO_4$ for the clean period, while 13.3% and 6.6% smaller than
313 those for the heavily polluted period, respectively. The results further confirmed that
314 substantial growth in the mass of NH_4NO_3 and $(NH_4)_2SO_4$ was an important reason
315 for the aerosol pollution. The formation of sulfate, nitrate, and ammonium (SNA) is
316 mainly affected by the emissions of precursors and the atmospheric oxidation capacity
317 Due to the great use of fossil fuel consumption, the emissions of precursors SO_2 and
318 NO_X per unit area in eastern China were estimated 2.3 and 3.4 times larger than the
319 national average, respectively (Cheng et al., 2012; Shi et al., 2014). Under high RH,
320 moreover, the SNA formation could significantly be elevated through gas-to-particle
321 heterogeneous reactions for the heavily polluted period (Seinfeld and Pandis, 2006).
322 Sulfate mass concentration, for example, increased from 6.4 μg/m^3 for the clean
323 period to 53.3 μg/m^3 for the heavily polluted period. Among all the size bins,
324 NH_4NO_3 and $(NH_4)_2SO_4$ were estimated to contribute the most to the mass
325 concentrations for 0.56-1.0 μm particles, with their mass fraction ranging 19.4-39.7%
326 and 18.1-34.7%, respectively, across different pollution levels. In comparison, the
327 largest contributions of OM appeared in the 0.056-0.18 μm fraction and were 31.2%,
328 29.0% and 52.3% for the clean, lightly polluted and heavily polluted periods,
329 respectively. As the largest PM fraction was found in the 0.56-1.0 μm size bin for the
330 heavily pollution period, the elevated concentrations of NH_4NO_3 and $(NH_4)_2SO_4$ in
331 $PM_{0.56-1.0}$ were the major causes of the increased aerosol pollution.

https://doi.org/10.5194/acp-2020-176
Preprint. Discussion started: 28 April 2020


Atmospheric Chemistry and Physics Discussions

Figure S4 in the Supplement compares the size distributions of PM mass concentrations and selected chemical species at the three sites. As mentioned above, a bimodal distribution with two peaks at 0.56-1.0 μm and 3.2-5.6 μm was observed for PM and OC at all the three sites, attributed to the coexistence of primary and secondary sources. Different from PAES and NUIST, NO_3^- had an obvious small coarse mode peak at NJU. Previous studies suggested that the chemistry of coarse mode NO_3^- can vary in different locations, and the components include NH_4NO_3, $NaNO_3$ and $Ca(NO_3)_2$ (Pakkanen et al., 1996). As NJU was close to the G25 highway, the reaction of HNO_3 with crustal particles could be an important process for coarse mode NO_3^- formation. The highest mean concentrations of NO_3^- and SO_4^{2-} at the 0.56-1.0 μm size among the three sites were observed at NJU, followed by NUIST and PAES. As NO_3^- and SO_4^{2-} were the major components of the aerosol light scattering, the variety of their mass concentrations at 0.56-1.0 μm could be a crucial reason for the visibility difference among the three sites. A greater difference was found for the size distribution of OC among the three sites, and the highest concentration at the 0.56-1.8 μm size was observed at NUIST. Our previous work found that NUIST was greatly influenced by VOCs emissions of surrounding industrial plants (Chen et al., 2019). Given its capability of light scattering and absorption, the abundant OC in the area could play an important role on the visibility.

3.2 Evaluation and optimization of the IMPROVE algorithm

Figure S5 in the Supplement presents the linear regressions between the measured daily aerosol scattering coefficients with the CAPS ($b_{sp\text{-}m}$) and those calculated with IMPROVE algorithms ($b_{sp\text{-}1999}$ and $b_{sp\text{-}2007}$) based on the measured concentrations of particle components at the three sites. At each site, strong correlations were found between the observation and IMPROVE estimation ($R^2 \geq 0.94$), indicating consistency between the different techniques. As shown in Figure S5a, the calculated aerosol scattering coefficients $b_{sp\text{-}1999}$ were 30%, 16% and 19% smaller than the measured values at NJU, PAES and NUIST, respectively. Similar results were found for other megacities in eastern China. Based on the online

https://doi.org/10.5194/acp-2020-176
Preprint. Discussion started: 28 April 2020


Atmospheric Chemistry and Physics Discussions

361 analytical methods, for example, Cheng et al. (2015) estimated that the scattering
362 coefficients predicted by the IMPROVE1999 algorithm were 34% smaller than the
363 measurement for a heavy pollution period in Shanghai. A greater underestimation of
364 the scattering coefficient existed at NJU than the other two sites, partly due to the
365 relatively abundance of sulfate and nitrate in particles at NJU. The sum of SO_4^{2-} and
366 NO_3^- accounted for 35.3 ± 13.2% of the total mass concentrations of $PM_{2.5}$ at NJU,
367 larger than the fraction at PAES (27.6 ± 12.9%) and NUIST (24.1 ± 11.6%) (note the
368 SO_4^{2-} and NO_3^- concentrations at the 0.56-1.0 μm were the largest at NJU as well, as
369 shown in Figure S4). Tao et al. (2014b) and Cheng et al. (2015) suggested that the
370 relatively small MSE of sulfate and nitrate aerosols in the IMPROVE1999 algorithm
371 might result in underestimation of the scattering coefficient in China, as sulfate and
372 nitrate were the main light-scattering components in $PM_{2.5}$.

373 As shown in Figure S5b, $b_{sp\text{-}2007}$ was only 4% smaller than the measurement at
374 NJU, and 4% and 18% larger at PAES and NUIST, respectively. Overall, the
375 performance of the IMPROVE2007 algorithm was better than that of the
376 IMPROVE1999, although deviation still existed due to the uncertainty in MSEs for
377 chemical species and the presence of light absorption organic matter such as BrC. A
378 relatively large deviation between $b_{sp\text{-}m}$ and $b_{sp\text{-}2007}$ was found at NUIST compared to
379 NJU and PAES. Chen et al. (2019) and Shao et al. (2016) found higher annual average
380 concentration of non-methane hydrocarbon at NUIST (34.4 ppbv) than NJU (22.0
381 ppbv) or PAES (27.1 ppbv). The more VOCs in the atmosphere were expected to
382 increase the SOC formation and to result in big deviation of $b_{sp\text{-}2007}$, as the OM with
383 light-absorption capability was not considered in IMPROVE2007.

384 Using the optimized IMPROVE algorithm as described in Section 2.4.1, the
385 aerosol scattering coefficients were recalculated and compared against the observation
386 at the three sites, as illustrated in Figure 2. Good correlations were found between the
387 observed and calculated scattering coefficients at all the sites ($R^2 \geq 0.96$), and the
388 regression slopes were estimated to be much closer to 1 than those between
389 observations and predictions with the IMPROVE1999 or IMPROVE2007 algorithms
390 (Figure S5). In addition, the MSEs calculated based on the Mie theory were applied to

https://doi.org/10.5194/acp-2020-176
Preprint. Discussion started: 28 April 2020


Atmospheric Chemistry and Physics Discussions

evaluate the results of the IMPROVE algorithms. As presented in Figure S6 in the Supplement, the MSEs of $(NH_4)_2SO_4$ and NH_4NO_3 calculated with the optimized IMPROVE algorithm were closer to the MSE simulated by Mie theory than those with the IMPROVE2007 algorithm. The results indicated the optimized algorithm had a better performance and could reduce the bias from the US IMPROVE algorithm.

As summarized in Table 2, the MSEs estimated with the optimized IMPROVE algorithm were 2.29, 4.82, 2.62, 5.35, 4.46, and 6.41 m^2/g for small sulfate, large sulfate, small nitrate, large nitrate, small and large OM, respectively. In comparison, the MSEs for the small and large size modes using the IMPROVE2007 were 2.2 and 4.8 m^2/g for $(NH_4)_2SO_4$, respectively, and 2.4 and 5.1 m^2/g for NH_4NO_3, respectively. The slightly larger MSEs from the optimized IMPROVE algorithm for $(NH_4)_2SO_4$ and NH_4NO_3 implied underestimation of the scattering coefficients of inorganic components when applying the previous algorithm. There were clear differences in the MSEs of OM (especially for fine OM) between the two algorithms, resulting from consideration of the light-absorbed OM in the optimized algorithm. Indicated by the m values in Table 2, the light-absorbed OC accounted for 66% and 71% of the fine MSOC mass at NJU and PAES, respectively, indicating that most of the fine MSOC had only light-absorption capacity. Unlike NJU and PAES, less than half of the fine MSOC (39%) had light-absorption capacity at NUIST, likely resulting from the varied sources of OM at the three sites. As described in our previous study (Chen et al., 2019), substantial OC was from the secondary formation in industrial polluted region, and its light-absorption capacity was weaker than that from the primary emissions.

Through field measurement and data reconstruction in different cities, previous studies explored the concentrations of $PM_{2.5}$ and its chemical components for various cities in China (Chen et al., 2019; Feng et al., 2012; Lai et al., 2016; Tao et al., 2013., Yang et al., 2011; Zhao et al., 2013). The major components of light scattering in aerosols, SNA, was found to typically account for half of the $PM_{2.5}$ mass concentrations in eastern Chinese cities like Nanjing, Shanghai, and Jinan (Yang et al., 2011). Given the similar level and strong regional transport of pollution among those cities, the optimized IMPROVE algorithm applied in Nanjing in this work is believed

https://doi.org/10.5194/acp-2020-176
Preprint. Discussion started: 28 April 2020


Atmospheric Chemistry and Physics Discussions

421 to be more suitable than the previous algorithms for eastern China.

422

423 **3.3 Effects of mixing state and relative humidity on aerosol light scattering**

424 Figure 3 presents the scattering coefficients measured by nephelometer and those
425 simulated by Mie theory at the three sites under dry conditions (RH < 40%). The
426 simulated scattering coefficients based on the assumption of an external mixing state
427 were larger than those based on core-shell and internal mixing states at all the three
428 sites. Compared with the internal and core-shell states, the simulated scattering
429 coefficients in the external mixing state were closer to the measurements at NJU and
430 PAES (Figure 3a and 3b), indicating the reasonable assumption of external mixtures
431 as the main mixing state of particles. Similarly, Ma et al. (2012) also suggested that
432 the external mixture was an important particle mixing state in northern China based
433 on a stochastic particle-resolved aerosol box model. Assuming the aerosol
434 components were externally mixed, Cheng et al. (2015) estimated the MSEs of
435 aerosol species in Shanghai, and found better agreement between the optimized
436 scattering coefficients and the measurements. At NUIST, the measured scattering
437 coefficients were closer to the simulated values in internal and core-shell states, likely
438 due to the high aging level of SOA at the industrial site (Figure 3c). Due to the strong
439 atmospheric oxidation and thereby the abundance of SOA coatings at NUIST, our
440 previous study suggested that the aerosol aging process could result in the growth of
441 internally mixed BC (Chen et al., 2019). Based on the observation of O_3 and
442 percentage of internally mixed BC, Lan et al. (2013) suggested that photochemical
443 production of secondary aerosol components was the main reason for the switching
444 from an external mixing state to an internal mixing state for BC.

445 In an actual environment, ambient aerosols are typically hygroscopic under the
446 conditions of high RH, and it is an important reason for visibility degradation. Table
447 S1 in the Supplement summarizes the growth factors (GF) of particle size measured in
448 Nanjing at different RH levels in previous studies. To evaluate the rationality of those
449 GF values, we followed the method by Tao et al. (2014b) and calculated the scattering
450 hygroscopic growth factor (f(RH)) at NJU based on the measured ambient scattering

https://doi.org/10.5194/acp-2020-176
Preprint. Discussion started: 28 April 2020


Atmospheric Chemistry and Physics Discussions

coefficients by CAPS and the dry scattering coefficients by nephelometer, as shown in Figure S7 in the Supplement. The correlation between f(RH) and RH was fitted through the power regression. Figure S8 in the Supplement presents a good agreement between the scattering coefficients estimated by f(RH) and those obtained by the Mie theory (R^2=0.95). The results indicate the accuracy of the GF values applied on different particle sizes and RH levels. The estimated and measured scattering coefficients at NJU under ambient condition are shown in Figure S9 in the Supplement. Different from the estimation under the dry conditions, the lowest value was found for the externally mixing state among the three mixing modes. In the externally mixing state, only sulfate and nitrate particles had hygroscopicity under wet conditions, whereas each particle had the capability of hygroscopic growth in the internal mixing and core-shell states, resulting in a significant increment in the scattering coefficient. Similarly, comparing the measured scattering coefficients under the dry and ambient conditions (Figure 3 and Figure S9), the simulated values based on an external mixing state were closer to the measurements than the other two modes, implying that RH had a limited effect on the particle mixing state.

To explore the impact of RH on the light scattering of particles with different sizes, the size distribution of f(RH) was estimate and shown in Figure 4. Large differences were found between f(RH) when the RH was above and below 75%, and high RH enhanced the capacity of scattering hygroscopicity growth of small size particles. Approximately 140 nm particles had strong hygroscopicity when the RH was below 75%, whereas a high f(RH) (1.41±0.03) was observed for the accumulation mode particles from 100 to 400 nm when the RH was above 75%. Similar results were reported for Beijing: larger hygroscopic GF was measured for accumulation mode particles (100–300 nm) with a hygroscopicity tandem differential mobility analyzer (H-TDMA), consistent with the elevated abundance of the light-scattering compositions such as sulfate and nitrate (Meier et al., 2009).

3.4 Size distribution of aerosol light scattering by pollution level

Figure 5 shows the size distribution of the scattering coefficients for particles and

https://doi.org/10.5194/acp-2020-176
Preprint. Discussion started: 28 April 2020


Atmospheric Chemistry and Physics Discussions

given chemical components under the three pollution levels. The scattering coefficients of particles for all size categories were the largest for the heavily polluted period (Figure 5a). The accumulation mode particles (0.18-1.8 μm) accounted for 92.9%, 92.6 and 93.4% of the total scattering coefficients for the clean, lightly polluted and heavily polluted periods, respectively. In particular, particles in the size bin of 0.56-1.0 μm accounted for 57% and 63% of the scattering coefficient for the heavily and lightly polluted periods, respectively, much larger than that for the clean period, 38%. From the results of Section 3.1, the abundance of particles of different sizes was considered to be an important factor for the variety of scattering coefficients across the whole size range.

As the dominant chemical components of aerosol light scattering, $(NH_4)_2SO_4$, NH_4NO_3 and OM collectively contributed 90%, 76% and 60% to the mass concentrations of $PM_{0.56\text{-}1.0}$ for the heavily polluted, lightly polluted and clean periods, respectively (Figure S2b-S2d). The scattering coefficients of $(NH_4)_2SO_4$ and NH_4NO_3 were the largest in the size bin of 0.56-1.0 μm for the three pollution levels, and their contributions increased along with the aggravation of pollution (Figure 5b and Figure 5c). The OM concentration in the size bin of 0.56-1.0 μm was 2.5 $\mu g/m^3$ for the clean period, and those for the lightly and heavily polluted periods were 160% and 510% larger, respectively. The scattering coefficient of OM in the size bin of 0.56-1.0 μm for the heavily polluted period was 15% less than that for the lightly polluted period, indicating the more important role of OM in the particle scattering effect for the lightly polluted period (Figure 5d). The large OM scattering contribution could likely be explained by the elevated mass fraction of OM and/or enhancement of the OM MSE. It could be inferred that the low visibility during heavy pollution resulted mainly from the enhancement of the scattering effect of SNA.

The MSEs of given chemical components in $PM_{1.8}$ are presented by pollution level in Figure 6. Increased MSEs for $(NH_4)_2SO_4$ and NH_4NO_3 were found along with the elevated $PM_{2.5}$ pollutions (Figure 6a). The large contributions of inorganic components and their strong light scattering ability were important reason for the reduced visibility during the heavily polluted period. Although the largest OM

https://doi.org/10.5194/acp-2020-176
Preprint. Discussion started: 28 April 2020


Atmospheric Chemistry and Physics Discussions

511 concentrations were observed in each size bin for the heavy pollution period, the
512 smallest MSE of OM in $PM_{1.8}$ was found for the heavily polluted period (3.73 m^2/g,
513 Figure 6b). As discussed in Section 3.2, most of the fine MSOC was expected to have
514 only a light-absorption effect whereas large MSOC had light-scattering capability.
515 With the optimized IMPROVE algorithm, the mass fraction of light-absorption OC to
516 total MSOC mass was estimated at 66.9±5.8% for the heavily polluted period, much
517 larger than those for clean and lightly polluted periods at 44.3±6.5% and 50.8±5.9%,
518 respectively, as shown in Figure S10 in the Supplement. Therefore, the small MSE of
519 OM for the heavily polluted period was partly attributed to the abundance of light
520 absorption BrC in $PM_{2.5}$.

521 For the whole research period, the MSEs of $(NH_4)_2SO_4$, NH_4NO_3 and OM in
522 $PM_{1.8}$ were calculated at 3.95, 4.26 and 4.14 m^2/g with the Mien theory, while the
523 analogue numbers in $PM_{2.5}$ were 3.94, 4.31 and 5.25 with the optimized IMPROVE
524 algorithm, respectively (Table 2). Very good agreement between the two methods was
525 found for SNA, and clearer discrepancy existed for OM, indicating a larger
526 uncertainty in the evaluation of organic aerosol scattering.

527

528 **3.5 Source apportionment of aerosol light scattering with the PMF-Mie coupled**
529 **model**

530 As illustrated in Figure 5, the light scattering of the accumulation mode (0.18-1.8
531 μm) accounted for the largest proportion of the total light scattering. To better
532 understand the causes of visibility degradation, the source apportionment of aerosol
533 light scattering at this size range was conducted for different pollution levels with the
534 PMF and Mie coupled model, as described in Section 2.4.2. The PMF model was
535 adopted to identify the potential sources and to estimate their respective contributions
536 to the mass concentration of accumulation mode particles. To resolve the appropriate
537 number of factors, different numbers of identifiable sources were tested. The results
538 of the source profiles and their contributions to accumulation mode particles at the
539 three sites are presented in Figure S11 in the Supplement and Figure 7a-c, respectively.
540 The main sources identified at the three sites include coal combustion, industrial

https://doi.org/10.5194/acp-2020-176
Preprint. Discussion started: 28 April 2020


Atmospheric Chemistry and Physics Discussions

pollution, vehicle, fugitive dust, biomass burning, and SIA (Figure S11). Compared to NJU and NUIST, vehicle contributed more to accumulated particles at the urban site PAES (Figure 7b). As stated in Section 2.4, we assumed that the contribution of the individual source category to the secondary particle component was proportional to the fraction of that source category to the emissions of corresponding precursors (Lang et al., 2017). Based on the emission inventory of precursors of SOC (VOCs) and SIA (NO_x, SO_2 and NH_3) in Nanjing (Huang, 2018), the source apportionment for primary and secondary particles of accumulation mode at the three sites were estimated, and the results are presented in Tables S2-S4 in the Supplement. With the source apportionment of secondary components, the contributions of coal combustion and industrial pollution increased 45-50% and 138-478% compared to those for primary particles across the three sites, respectively. The result indicates that the gaseous precursors from coal combustion and industrial pollution greatly elevate the aerosol pollution.

The contributions of different aerosol species to the aerosol light scattering were estimated using the Mie model, and the results are presented in Table S5 in the Supplement. OM contributed the most to the total scattering at the three sites (31%, 29% and 33% for NJU, PAES and NUIST, respectively). Compared to other Chinese mega cities, the contribution of OM in Nanjing was close to that for inland cities like Beijing (Tao et al., 2015) and Tianjin (Wang et al., 2016b), but was much larger than that observed in a coastal megacity, Guangzhou (Tao et al., 2014c).

Combined with the source apportionment from the PME model, Figure 7d-7f illustrates the source contribution to aerosol light scattering at the three sites. Coal combustion, industrial plants and vehicle were the major sources of the aerosol light scattering in Nanjing, and the three source categories collectively accounted for 64-70% of the total scattering capacity of aerosols. Given their relatively intensive activities in urban and industrial regions, vehicles and industrial plants were identified as the largest contribution sources at PAES and NUIST, respectively. Indicated by the dashed lines in Figure 7d-7f, the collective contributions of secondary aerosol components were estimated to be 26.7%-35.2% of the total scattering at the three sites,

https://doi.org/10.5194/acp-2020-176
Preprint. Discussion started: 28 April 2020


Atmospheric Chemistry and Physics Discussions

571 suggesting the important role of secondary aerosol formation in visibility reduction.

572 Figure 8 illustrates the source apportionment of aerosol light scattering for the
573 clean and polluted periods at the three sites. Coal combustion contributed the most to
574 the total scattering for the clean period, and the contribution declined significantly for
575 the polluted period, from 39% to 21%, from 38% to 19% and from 35% to 18% at
576 NJU, PAES and NUIST, respectively. The results implied that coal combustion might
577 not be the most important reason for visibility degradation in polluted periods.
578 Similarly, the contribution of fugitive dust during the polluted period was estimated to
579 be smaller than that for the clean condition. In contrast, the contributions of vehicles
580 and industrial pollution to light scattering increased from 27% to 48%, from 27% to
581 47% and from 31% to 62% for the polluted periods compared to the clean period at
582 NJU, PAES, and NUIST, respectively. As shown in Figure 8b and 8c, particularly, the
583 contribution of primary emissions from vehicles to aerosol scattering was estimated to
584 increase from 11.4% to 21.5% at PAES, and that from industrial plants increased from
585 4.5% to 13.5% at NUIST. The primary aerosol emissions from vehicles and industrial
586 plants were thus identified as the main cause of visibility reduction in the urban and
587 industrial areas, respectively. Similarly, Wang et al. (2016b) suggested that vehicle
588 was the dominate source of aerosol light extinction in Hangzhou, with the
589 contribution to the total extinction coefficient of $PM_{2.5}$ reaching 30.2%. The present
590 study indicated that more effective measures for reducing the primary particle
591 emissions from vehicles and industrial production should be conducted to avoid
592 severe haze pollution in urban and industrial regions.

593 In addition, the results suggest that secondary aerosols were another important
594 contributor to the reduced visibility. From the clean to the heavily polluted periods, as
595 shown in Figure 8, the contributions of secondary aerosols to the total light scattering
596 increased from 19.9% to 36.7%, from 20.9% to 32.4%, and from 28.6% to 41.7% at
597 NJU, PAES, and NUIST, respectively. As shown in Table 3, the contributions of SIA
598 to the total scattering at the three sites were ranged at 14.5%-19.9% and 24.5%-28.0%,
599 much more than those of SOA at 4.1%-8.7% and 7.9%-13.7% for the clean and
600 polluted periods, respectively. The results imply that SIA had a greater impact on

https://doi.org/10.5194/acp-2020-176
Preprint. Discussion started: 28 April 2020


Atmospheric Chemistry and Physics Discussions

visibility degradation. Although the contribution of coal combustion to the total scattering declined from clean to polluted periods, the contributions of SIA from coal combustion for the polluted periods were 88%, 35% and 36% larger than those for the clean period at NJU, PAES and NUIST, respectively. The enhancement of SIA from coal combustion was thus an important cause of polluted days. Moreover, the contribution of SOA to the total scattering coefficient during the polluted periods was estimated at 13.7% at NUIST, larger than the 7.9% and 9.1% at PAES and NJU, respectively, indicating that the contribution of SOA to visibility reduction at industrial polluted areas should not be ignored. Notably, there is uncertainty in the methodology of source apportionment of aerosol scattering coefficients. In particular, the assumption that the secondary components were proportional to the emissions of their precursors is a simplified method and probably led to large bias, as the complicated nonlinear mechanism of secondary aerosol formation is not recognized. More tools including chemistry transport modeling and radiocarbon measurements are thus recommended to be integrated into future studies to better determine the primary and secondary sources of aerosols.

4 CONCLUSIONS

A comprehensive investigation of the light-scattering properties of atmospheric aerosols was conducted from November 2015 to March 2017 at three functional sites in Nanjing. High concentrations of sulfate and nitrate in $PM_{0.56\text{-}1.0}$ were the major causes of the heavy particle pollution events. The varied abundance of secondary inorganic components at the three sites was an important reason for the visibility differences, and OC played an important role on the visibility reduction in the industrial area due to its complicated optical effect. Based on the measured aerosol scattering coefficients and the mass concentrations of aerosol components, an optimized algorithm of IMPROVE that considered the light absorption effect of OM was developed to better represent the aerosol optical property.

Compared with internal and core-shell mixing states, the simulated scattering coefficients based on an external mixing assumption were closer to the measurements

https://doi.org/10.5194/acp-2020-176
Preprint. Discussion started: 28 April 2020

Atmospheric Chemistry and Physics Discussions

at NJU and PAES, indicating that externally mixed particles widely existed at urban and suburban areas. At the industrial site NUIST, the high aging level of SOA was the main reason for particle switching from external to internal mixing states. The results for the scattering coefficients under dry and ambient conditions indicated that RH had little effect on particle mixing state but a large impact on the scattering coefficients. Particles in the size range of 0.56-1.0 μm contributed the most (38%-63%) to the total scattering coefficient under different pollution levels. As the dominant light scattering species in aerosols, NH_4NO_3, $(NH_4)_2SO_4$ and OM collectively contributed 90%, 81% and 76% of the mass concentrations of $PM_{0.56\text{-}1.0}$ for the heavily polluted, lightly polluted and clean periods, respectively. The low visibility during the heavy pollution period mainly resulted from the enhanced light scattering of SNA. The abundance of light-absorption OC was an important reason for the relatively low contribution of OM to light scattering in the heavy pollution period.

Through a coupled model of PMF and Mie theory, we found coal combustion, industrial plants and vehicle were the main sources of the visibility reduction in Nanjing. Vehicles and industrial plants were the main causes for visibility reduction in urban and industrial areas, respectively. The increased emissions of SIA precursors from coal combustion were an important cause of polluted days, and the contribution of SOA to visibility reduction at industrial pollution areas should not be ignored. The source apportionment of aerosol light scattering in this work provides scientific evidence for the control of haze pollution in different functional areas of cities in developed eastern China.

DATA AVAILABILITY

All data in this study are available from the authors upon request.

https://doi.org/10.5194/acp-2020-176
Preprint. Discussion started: 28 April 2020

Atmospheric Chemistry and Physics Discussions

AUTHOR CONTRIBUTIONS

DC developed the strategy and methodology of the work and wrote the draft. YZ improved the methodology and revised the manuscript. JZ, HY and XY provided observation data of aerosol scattering coefficient.

COMPETING INTERESTS

The authors declare that they have no conflict of interest.

ACKNOWLEDGEMENT

This work was sponsored by the Natural Science Foundation of China (41922052 and 91644220), and the National Key Research and Development Program of China (2017YFC0210106).

REFERENCES

Alexander, D. T. L., Crozier, P. A., Anderson, J. R.: Brown carbon spheres in East Asian outflow and their optical properties, Science, 321, 833-836, doi:10.1126/science.1155296, 2008.

Andreae, M. O., Schmid, O., Yang, H., Chand, D., Yu, J. Z., Zeng, L. M., Zhang, Y. H.: Optical properties and chemical composition of the atmospheric aerosol in urban Guangzhou, China, Atmos. Environ., 42, 6335-6350, doi:10.1016/j.atmosenv.2008.01.030, 2008.

Bohren, C. F, Huffman, D. R.: Absorption and scattering of light by small particles [R], New York: Wiley, Inc., 1998.

Bond, T. C., Bergstrom, R. W.: Light Absorption by Carbonaceous Particles: An Investigative Review, Aerosol Sci. Technol., 40, 27-67, doi:10.1080/02786820500421521, 2006.

Cao, J. J., Lee, S. C., Chow, J. C., Watson, J. G., Ho, K. F., Zhang, R. J., Jin, Z. D., Shen, Z. X., Chen, G. C., Kang, Y. M., Zou, S. C., Zhang, L. Z., Qi, S. H., Dai, M. H.,

https://doi.org/10.5194/acp-2020-176
Preprint. Discussion started: 28 April 2020


Atmospheric Chemistry and Physics Discussions

683 Cheng, Y., Hu, K.: Spatial and seasonal distributions of carbonaceous aerosols over
684 China, J. Geophys. Res., 112, D22S11, doi:10.1029/2006JD008205, 2007.
685 Cao, J. J., Wang, Q. Y., Chow, J. C., Watson, J. G., Tie, X. X., Shen, Z. X., Wang, P.,
686 An, Z. S.: Impacts of aerosol compositions on visibility impairment in Xi'an, China,
687 Atmos. Environ., 59, 559-566, doi:10.1016/j.atmosenv.2012.05.036, 2012.
688 Chen, D., Cui, H., Zhao, Y., Yin, L., Lu, Y., Wang, Q.: A two-year study of
689 carbonaceous aerosols in ambient $PM_{2.5}$ at a regional background site for western
690 Yangtze River Delta, China, Atmos. Res., 183, 351-361,
691 doi:10.1016/j.atmosres.2016.09.004, 2017.
692 Chen, D., Zhao, Y., Lyu, R., Wu, R., Dai, L., Zhao, Y., Chen, F., Zhang, J., Yu, H.,
693 Guan, M.: Seasonal and spatial variations of optical properties of light absorbing
694 carbon and its influencing factors in a typical polluted city in Yangtze River Delta,
695 China, Atmos. Environ., 199, 45-54, doi:10.1016/j.atmosenv.2018.11.022, 2019.
696 Cheng, M. C., You, C. F., Cao, J., Jin, Z.: Spatial and seasonal variability of water
697 soluble ions in PM2.5 aerosols in 14 major cities in China, Atmos. Environ., 60,
698 182-192, 10.1016/j.atmosenv.2012.06.037, 2012.
699 Cheng, Y., He, K.B., Du, Z.Y., Engling, G., Liu, J.M., Ma, Y.L., Zheng, M., Weber,
700 R.J.: The characteristics of brown carbon aerosol during winter in Beijing, Atmos.
701 Environ., 127, 355-364, doi:10.1016/j.atmosenv.2015.12.035, 2016.
702 Cheng, Y., He, K.B., Engling, G., Weber, R., Liu, J.M., Du, Z.Y., Dong, S.P.: Brown
703 and black carbon in Beijing aerosol: Implications for the effects of brown coating on
704 light absorption by black carbon, Sci. Total Environ., 599–600, 1047-1055.
705 doi:10.1016/j.scitotenv.2017.05.061, 2017.
706 Cheng, Z., Jiang, J., Chen, C., Gao, J., Wang, S., Watson, J.G., Wang, H., Deng, J.,
707 Wang, B., Zhou, M.: Estimation of aerosol mass scattering efficiencies under high
708 mass loading: case study for the megacity of Shanghai, China, Environ. Sci. Technol.,
709 49, 831-838, doi:10.1021/es504567q, 2015.
710 Ding, J., Han, S., Zhang, Y., Feng, Y., Wu, J., Shi, G., Wang, J.: Chemical
711 characteristics of particles and light extinction effects in winter in Tianjin, Res.
712 Environ. Sci., 28, 1353-1361, doi:10.13198/j.issn.1001-6929.2015.09.03, 2015.

https://doi.org/10.5194/acp-2020-176
Preprint. Discussion started: 28 April 2020


Atmospheric Chemistry and Physics Discussions

713 Feng, J. L., Sun, P., Hu, X. L., Zhao, W., Wu, M. H., Fu, J. M.: The chemical
714 composition and sources of PM2.5 during the 2009 Chinese New Year's holiday in
715 Shanghai, Atmos. Res., 118, 435-444, doi:10.1016/j.atmosres.2012.08.012, 2012.
716 Huang, R. J., Yang, L., Cao, J., Chen, Y., Chen, Q., Li, Y., Duan, J., Zhu, C., Dai, W.,
717 Wang, K.: Brown Carbon Aerosol in Urban Xi'an, Northwest China: The Composition
718 and Light Absorption Properties, Environ. Sci. Technol., 52, 6825-6833,
719 doi:10.1021/acs.est.8b02386, 2018.
720 Huang, Y.W: Effects of changes in emission and meteorological conditions on fine
721 particulate levels in the city scale, Master thesis, Nanjing University, 2018.
722 Hueglin, C., Gehrig, R., Baltensperger, U., Gysel, M., Monn, C., and Vonmont, H.:
723 Chemical characterisation of PM2.5, PM10 and coarse particles at urban, near-city
724 and rural sites in Switzerland, Atmos. Environ., 39, 637–651,
725 doi:10.1016/j.atmosenv.2004.10.027, 2005.
726 Jacobson, M.Z.: Strong radiative heating due to the mixing state of black carbon in
727 atmospheric aerosols, Nature, 409, 695-697, doi:10.1038/35055518, 2001.
728 Khan, M. F., Latif, M. T., Hwa, S. W., Amil, N., Nadzir, M. S. M., Sahani, M., Tahir,
729 N. M., Jing, X. C.: Fine particulate matter in the tropical environment: monsoonal
730 effects, source apportionment, and health risk assessment, Atmos. Chem. Phys., 16,
731 597-617, doi:10.5194/acp-16-597-2016, 2016.
732 Kim, E., Hopke, P.K.: Improving source identification of fine particles in a rural
733 northeastern US area utilizing temperature-resolved carbon fractions, J. Geophys.
734 Res.: Atmos., 109, D09204, doi:10.1029/2003jd004199, 2004.
735 Lai, S.C.: Characterization of PM2.5 and the major chemical components during a
736 1-year campaign in rural Guangzhou, Southern China, Atmos. Res., 167, 208-215,
737 doi:10.1016/j.atmosres.2015.08.007, 2016.
738 Lan, Z. J., Huang, X. F., Yu, K. Y., Sun, T. L., Zeng, L. W., Hu, M.: Light absorption
739 of black carbon aerosol and its enhancement by mixing state in an urban atmosphere
740 in South China, Atmos. Environ., 69, 118-123, doi:10.1016/j.atmosenv.2012.12.009,
741 2013.
742 Lang, J. L., Cheng, S. Y., Wen, W., Liu, C., Wang, G.: Development and application of

https://doi.org/10.5194/acp-2020-176
Preprint. Discussion started: 28 April 2020


Atmospheric Chemistry and Physics Discussions

743 a new $PM_{2.5}$ source apportionment approach, Aerosol Air Qual. Res., 17, 340-350, doi:
744 10.4209/aaqr.2015.10.0588, 2017.
745 Lei, Y., Shen, Z., Wang, Q., Zhang, T., Cao, J., Sun, J., Zhang, Q., Wang, L., Xu, H.,
746 Tian, J., 2018. Optical characteristics and source apportionment of brown carbon in
747 winter PM2.5 over Yulin in Northern China, Atmos. Res., 213, 27-33,
748 doi:10.1016/j.atmosres.2018.05.018, 2018.
749 Li, B., Zhang, J., Zhao, Y., Yuan, S., Zhao, Q., Shen, G., Wu, H.: Seasonal variation of
750 urban carbonaceous aerosols in a typical city Nanjing in Yangtze River Delta, China,
751 Atmos. Environ., 106, 223-231, doi:10.1016/j.atmosenv.2015.01.064, 2015.
752 Liu, X., Cheng, Y., Zhang, Y., Jung, J., Sugimoto, N., Chang, S. Y., Kim, Y. J., Fan, S.,
753 Zeng, L.: Influences of relative humidity and particle chemical composition on
754 aerosol scattering properties during the 2006 PRD campaign, Atmos. Environ., 42,
755 1525-1536, doi:10.1016/j.atmosenv.2007.10.077, 2008.
756 Liu, H. J., Zhao, C. S., Nekat, B., Ma, N., Herrmann, H.: Aerosol hygroscopicity
757 derived from size-segregated chemical composition and its parameterization in the
758 North China Plain, Atmos. Chem. Phys., 14, 2525-2539,
759 doi:10.5194/acp-14-2525-2014, 2014.
760 Liu, D., Whitehead, J., Alfarra, M. R., Reyesvillegas, E., Spracklen, D. V., Reddington,
761 C. L., Kong, S., Williams, P. I., Ting, Y. C., Haslett, S.: Black-carbon absorption
762 enhancement in the atmosphere determined by particle mixing state, Nature Geosci.,
763 10, 184-188, doi:10.1038/ngeo2901, 2017.
764 Lowenthal, D. H., Naresh, K.: PM2.5 mass and light extinction reconstruction in
765 IMPROVE, J. Air Waste Manag. Assoc., 53, 1109-1120,
766 doi:10.1080/10473289.2003.10466264, 2003.
767 Ma, N., Zhao, C. S., Müller, T., Cheng, Y. F., Liu, P. F., Deng, Z. Z., Xu, W. Y., Ran,
768 L., Nekat, B., Van Pinxteren, D., Gnauk, T., Müller, K., Herrmann, H., Yan, P., Zhou,
769 X.J., Wiedensohler, A.: A new method to determine the mixing state of light absorbing
770 carbonaceous using the measured aerosol optical properties and number size
771 distributions, Atmos. Chem. Phys., 12, 2381-2397, doi:10.5194/acp-12-2381-2012,
772 2012.

https://doi.org/10.5194/acp-2020-176
Preprint. Discussion started: 28 April 2020


Atmospheric Chemistry and Physics Discussions

773 Malm, W.C., Hand, J. L.: An examination of the physical and optical properties of
774 aerosols collected in the IMPROVE program, Atmos. Environ., 41, 3407-3427,
775 doi:10.1016/j.atmosenv.2006.12.012, 2007.
776 Meier, J., Wehner, B., Massling, A., Birmili, W., Nowak, A., Gnauk, T., Bruggemann,
777 E., Herrmann, H., Min, H., Wiedensohler, A.: Hygroscopic growth of urban aerosol
778 particles in Beijing (China) during wintertime: a comparison of three experimental
779 methods, Atmos. Chem. Phys., 9, 6865-6880, doi:10.5194/acp-9-6889-2009, 2009.
780 Ministry of Environmental Protection of China (MEP): Technical regulation on
781 ambient air quality index, China Environ.Sci. Press, HJ633-2012, 2012.
782 Moon, K. J., Han, J. S., Ghim, Y. S., Kim, Y. J.: Source apportionment of fine
783 carbonaceous particles by positive matrix factorization at Gosan background site in
784 East Asia, Environ. Int., 34, 654-664, doi:10.1016/j.envint.2007.12.021, 2008.
785 Onasch, T. B., Massoli, P., Kebabian, P. L., Hills, F. B., Bacon, F. W., Freedman, A.:
786 Single Scattering Albedo Monitor for Airborne Particulates, Aerosol Sci. Technol., 49,
787 267-279, doi:10.1080/02786826.2015.1022248, 2015.
788 Pakkanen, T. A., Kerminen, V. M., Hillamo, R. E., Makinen, M., Makela, T., and
789 Virkkula, A.: Distribution of nitrate over seasalt and soil derived particles implications
790 from a field study, J. Atmos. Chem., 24, 189–205, 1996.
791 Petzold, A., Onasch, T., Kebabian, P., Freedman, A.: Intercomparison of a Cavity
792 Attenuated Phase Shift-based extinction monitor (CAPS PMex) with an integrating
793 nephelometer and a filter-based absorption monitor, Atmos. Meas. Tech., 6,
794 1141-1151, doi:10.5194/amt-6-1141-2013, 2013.
795 Pitchford, M., Malm, W., Schichtel, B., Kumar, N., Lowenthal, D., Hand, J.: Revised
796 algorithm for estimating light extinction from IMPROVE particle speciation data, J.
797 Air Waste Manag. Assoc., 57, 1326-1336, doi:10.3155/1047-3289.57.11.1326, 2007.
798 Ramanathan, V., Li, F., Ramana, M. V., Praveen, P. S., Kim, D., Corrigan, C. E.,
799 Nguyen, H., Stone, E. A., Schauer, J. J., Carmichael, G. R., Adhikary, B., Yoon, S. C.:
800 Atmospheric brown clouds: Hemispherical and regional variations in long-range
801 transport, absorption, and radiative forcing, J. Geophys. Res.: Atmos., 112, D22S21,
802 doi:10.1029/2006JD008124, 2007.

https://doi.org/10.5194/acp-2020-176
Preprint. Discussion started: 28 April 2020

803 Schwartz, S.: The Whitehouse Effect–Shortwave radiative forcing of climate by
804 anthropogenic aerosols: An overview, J. Aerosol Sci., 27, 359–382,
805 doi:10.1016/0021-8502(95)00533-1, 1996.
806 Seinfeld, J. H., Pandis.: Atmospheric chemistry and physics: From air pollution to
807 climate change, doi:10.1080/00139157.1999.10544295, 2006.
808 Shao, P., An, J., Xin, J., Wu, F., Wang, J., J, D., Wang, Y.: Source apportionment of
809 VOCs and the contribution to photochemical ozone formation during summer in the
810 typical industrial area in the Yangtze River Delta, China, Atmos. Res., 176-177, 64-74,
811 doi:10.1016/j.atmosres.2016.02.015, 2016.
812 Shi, Y., Chen, J., Hu, D., Wang, L., Yang, X., Wang, X.: Airborne submicron
813 particulate (PM1) pollution in Shanghai, China: chemical variability,
814 formation/dissociation of associated semi-volatile components and the impacts on
815 visibility, Sci. Total Environ., 473, 199-206, 10.1016/j.scitotenv.2013.12.024, 2014.
816 Swietlicki, E., Hansson, H. C., Hämeri, K., Svenningsson, B., Massling, A.,
817 McFiggans, G., McMurry, P. H., Petäjä, T., Tunved, P., Gysel, M., Topping, D.,
818 Weingartner, E., Baltensperger, U., Rissler, J., Wiedensohler, A., Kulmala, M.:
819 Hygroscopic properties of submicrometer atmospheric aerosol particles measured
820 with H-TDMA instruments in various environments – a review, Tellus B, 60, 432–469,
821 doi:10.1111/j.1600-0889.2008.00350.x, 2008.
822 Tang, I. N.: Chemical and size effects of hygroscopic aerosols on light scattering
823 coefficients, J. Geophys. Res.: Atmos., 101, 19245-19250, doi:10.1029/96jd03003,
824 1996.
825 Tao, J., Cheng, T., Zhang R.: Chemical composition of PM2.5 at an urban site of
826 Chengdu in southwestern China, Adv. Atmos. Sci., 30, 1070-1084,
827 doi:10.1007/s00376-012-2168-7, 2013.
828 Tao, J. C , Zhao, C. S., Ma, N., Liu, P. F.: The impact of aerosol hygroscopic growth
829 on the single-scattering albedo and its application on the NO_2 photolysis rate
830 coefficient, Atmos. Chem. Phys., 14, 12055-12067, doi:10.5194/acp-14-12055-2014,
831 2014a.
832 Tao, J., Zhang, L., Cao, J., Hsu, S. C., Xia, X., Zhang, Z., Lin, Z., Cheng, T., Zhang,

https://doi.org/10.5194/acp-2020-176
Preprint. Discussion started: 28 April 2020

R.: Characterization and source apportionment of aerosol light extinction in Chengdu, southwest China, Atmos. Environ., 95, 552-562, doi:10.1016/j.atmosenv.2014.07.017, 2014b.

Tao, J., Zhang, L., Kinfai, H. O., Zhang, R., Lin, Z., Zhang, Z., Lin, M., Cao, J., Liu, S., Wang, G.: Impact of $PM_{2.5}$ chemical compositions on aerosol light scattering in Guangzhou - the largest megacity in South China, Atmos. Res., 135-136, 48-58, doi:10.1016/j.atmosres.2013.08.015, 2014c.

Tao. J., Zhang, L., Gao. J., Wang. H., Chai. F., Wang. S: Aerosol chemical composition and light scattering during a winter season in Beijing, Atmos. Environ., 110, 36-44, doi:10.1016/j.atmosenv.2015.03.037, 2015.

Tian, S. L., Pan, Y. P., Wang, Y. S.: Size-resolved source apportionment of particulate matter in urban Beijing during haze and non-haze episodes, Atmos. Chem. Phys., 15, 9405-9443, doi:10.5194/acp-15-9405-2015, 2015.

Titos, G., Cazorla, A., Zieger, P., Andrews, E., Lyamani, H., Granados-Muñoz, M. J., Olmo, F. J., Alados-Arboledas, L.: Effect of hygroscopic growth on the aerosol light-scattering coefficient: A review of measurements, techniques and error sources, Atmos. Environ., 141, 494-507, doi:10.1016/j.atmosenv.2016.07.021, 2016.

Wang, H., An, J., Cheng, M., Shen, L., Zhu, B., Li, Y., Wang, Y., Duan, Q., Sullivan, A., Xia, L.: One year online measurements of water-soluble ions at the industrially polluted town of Nanjing, China: Sources, seasonal and diurnal variations, Chemosphere, 148, 526-536, doi:10.1016/j.chemosphere.2016.01.066, 2016a.

Wang. J., Zhang, Y., Feng, Y., Zheng, X., Li, J., Hong, S., Shen, J., Tan, Z., Jing, D., Qi, Z.: Characterization and source apportionment of aerosol light extinction with a coupled model of CMB-IMPROVE in Hangzhou, Yangtze River Delta of China, Atmos. Res., 178-179, 570-579, doi:10.1016/j.atmosres.2016.05.009, 2016b.

Wang, S. R., Yu, Y. Y., Wang, Q. G., Lu, Y., Yin, L. N., Zhang, Y. Y., Lu, X. B.: Source apportionment of $PM_{2.5}$ in Nanjing by PMF, China Environ.Sci., 35, 3535-3542, 2015.

Watson, J. G.: Visibility: Science and regulation, J. Air Waste Manage. Assoc., 52, 628-713, 2002.

Watson, J. G., Chow, J. C., Lowenthal, D. H., L-W, A. C., Stephanie, S., Edgerton, E.

https://doi.org/10.5194/acp-2020-176
Preprint. Discussion started: 28 April 2020


Atmospheric Chemistry and Physics Discussions

S., Blanchard, C. L.: $PM_{2.5}$ source apportionment with organic markers in the Southeastern Aerosol Research and Characterization (SEARCH) study, J. Air Waste Manage. Assoc., 65, 1104-1118, doi:10.1080/10962247.2015.1063551, 2015.

Xu, J., Bergin, M. H., Yu, X., Liu, G., Zhao, J., Carrico, C. M., Baumann, K.: Measurement of aerosol chemical, physical and radiative properties in the Yangtze delta region of China, Atmos. Environ., 36, 161-173, doi:10.1016/s1352-2310(01)00455-1, 2002.

Xu, J., Tao, J., Zhang, R., Cheng, T., Leng, C., Chen, J., Huang, G., Li, X., Zhu, Z.: Measurements of surface aerosol optical properties in winter of Shanghai, Atmos. Res., 109-110, 25-35, doi:10.1016/j.atmosres.2012.02.008, 2012.

Xue, L., Ding, A., Gao, J., Wang, T., Wang, W., Wang, X., Lei, H., Jin, D., Qi, Y.: Aircraft measurements of the vertical distribution of sulfur dioxide and aerosol scattering coefficient in China, Atmos. Environ., 44, 278-282, doi:10.1016/j.atmosenv.2009.10.026, 2010.

Yan, C. Q., Zheng, M., Zhang, Y. H.: Research progress and direction of atmospheric brown carbon, Environ. Sci., 35, 4404-4414, doi:10.13227/j.hjkx.2014.11.050, 2014.

Yang, F., Tan, J., Zhao, Q., Du, Z., He, K., Ma, Y., Duan, F., Chen, G., Zhao, Q.: Characteristics of $PM_{2.5}$ speciation in representative megacities and across China, Atmos. Chem. Phys., 11, 5207-5219, doi:10.5194/acp-11-5207-201, 2011.

Zhang, L., Sun, J. Y., Shen, X. J., Zhang, Y. M., Che, H. C., Ma, Q. L., Zhang, Y. W., Zhang, X. Y., Ogren, J. A.: Observations of relative humidity effects on aerosol light scattering in the Yangtze River Delta of China, Atmos. Chem. Phys., 15, 2853-2904, doi:10.5194/acp-15-8439-2015, 2015.

Zhang, Y., Forrister, H., Liu, J., Dibb, J., Anderson, B., Schwarz, J. P., Perring, A. E., Jimenez, J. L., Campuzanojost, P., Wang, Y.: Top-of-atmosphere radiative forcing affected by brown carbon in the upper troposphere, Nature Geosci., 10, doi:10.1038/ngeo2960, 2017.

Zhao, P. S., Dong, F., He, D., Zhao, X. J., Zhang, W. Z., Yao, Q., Liu, H. Y.: Characteristics of concentrations and chemical compositions for PM2.5 in the region of Beijing, Tianjin, and Hebei, China, Atmos. Chem. Phys., 13, 4631-4644.

https://doi.org/10.5194/acp-2020-176
Preprint. Discussion started: 28 April 2020

Atmospheric Chemistry and Physics Discussions

893 doi:10.5194/acp-13-4631-2013, 2013.

894 Zhao, Y., Qiu, L. P., Xu, R., Xie, F., Zhang, Q., Y. Yu, Y., Nielsen, C. P., Qin, H.,
895 Wang, H., Wu, X., Q. Li, W., Zhang, J.: Advantages of a city-scale emission inventory
896 for urban air quality research and policy: the case of Nanjing, a typical industrial city
897 in the Yangtze River Delta, China, Atmos. Chem. Phys., 15, 12623-12644.
898 doi:10.5194/acpd-15-18691-2015, 2015.

899

https://doi.org/10.5194/acp-2020-176
Preprint. Discussion started: 28 April 2020

Atmospheric Chemistry and Physics Discussions

FIGURE CAPTIONS

Figure 1. The mass concentrations and fractions of the main chemical components of particles with different sizes in Nanjing on clean, lightly-polluted and heavily-polluted days during the sampling period.

Figure 2. Linear regressions between the measured light scattering coefficients and those estimated with the optimized IMPROVE algorithm at NJU, PAES, NUIST and all three sites.

Figure 3. The comparison of measured and estimated dry scattering coefficients based on the assumptions of external, internal, and core-shell mixture at NJU (a), PAES (b) and NUIST (c).

Figure 4. The size distribution of hygroscopic scattering growth of particles under varied relative humidity levels at the three sites.

Figure 5. The size distribution of scattering coefficients of aerosol particles (a), $(NH_4)_2SO_4$ (b), NH_4NO_3 (c) and OM (d) under different pollution levels. The contributions of particles with different sizes to total scattering coefficient are indicated in the panels as well.

Figure 6. The size distribution of mass concentrations of $(NH_4)_2SO_4$, NH_4NO_3 (a), and OM (b) under different pollution levels and mass scattering efficiencies (MSE) for $PM_{1.8}$. The size of dot represents the MSEs of $PM_{1.8}$ (Unit: m^2/g).

Figure 7. Source apportionment of accumulation mode particles at NJU (a), PAES (b) and NUIST (c), and source apportionment of light scattering for accumulation mode particles at NJU (d), PAES (e) and NUIST (f). The shadow represents the contribution of secondary aerosols from each source category.

Figure 8. Source apportionment of light scattering for accumulation mode particles for the clean and polluted periods at NJU (a), PAES (b) and NUIST (c). The shadow represents the contribution of secondary aerosols from each source category.

https://doi.org/10.5194/acp-2020-176
Preprint. Discussion started: 28 April 2020

Atmospheric Chemistry and Physics Discussions

928 **TABLES**

929 **Table 1. The concentrations of particulate matter and its chemical components**
930 **(μg/m^3), light scattering coefficients (Mm^{-1}), and selected meteorological**
931 **parameters including wind speed (WS, m/s) and relative humidity (RH, %) at all**
932 **the three sites for different pollution levels from November 2015 to January**
933 **2017.**

Category	Clean period	Lightly polluted period	Heavily polluted period
AQI	65.8 ± 15.7	110.6 ± 21.3	209.4 ± 30.1
PM_{10}	80.4 ± 26.3	143.1 ± 28.6	244.2 ± 21.2
$PM_{2.5}$	47.9 ± 15.8	102.1 ± 16.4	163.1 ± 13.6
OC	8.6 ± 3.2	14.2 ± 3.2	27.6 ± 5.0
EC	1.9 ± 0.9	3.0 ± 1.2	5.3 ± 0.1
SO_4^{2-}	6.9 ± 3.9	13.5 ± 5.6	33.8 ± 9.2
NO_3^-	10.5 ± 5.4	22.7 ± 8.7	47.9 ± 17.7
Cl^-	1.8 ± 1.5	2.2 ± 1.3	4.8 ± 1.4
Ca^{2+}	1.2 ± 0.8	1.3 ± 1.6	0.8 ± 0.1
Na^+	0.8 ± 0.2	0.9 ± 0.3	1.0 ± 0.1
Mg^{2+}	0.1 ± 0.1	0.2 ± 0.1	0.1 ± 0.0
NH_4^+	5.1 ± 1.9	9.2 ± 2.2	16.9 ± 2.5
K^+	0.9 ± 0.2	1.3 ± 0.3	2.1 ± 0.7
CO	0.8 ± 0.2	1.3 ± 0.3	1.6 ± 0.1
NO_2	57.4 ± 18.0	71.6 ± 20.0	91.2 ± 32.8
SO_2	17.7 ± 6.5	21.1 ± 6.0	29.5 ± 12.5
WS	1.6 ± 0.3	1.4 ± 0.5	1.0 ± 0.3
RH	56.1 ±13.5	62.7 ± 10.8	68.9 ± 4.9
b_{sp}	251.4 ± 170.8	558.3 ± 236.4	1286.2 ± 293.3

934

https://doi.org/10.5194/acp-2020-176
Preprint. Discussion started: 28 April 2020

Atmospheric Chemistry and Physics Discussions

935 **Table 2. The mass scattering efficiencies (MSEs, m^2/g) of chemical species in the**
936 **optimized and the existing algorithms from the Interagency Monitoring of**
937 **Protected Visual Environments (IMPROVE). The sample numbers and the mass**
938 **fractions of light-absorption BrC to MSOC for small and large size modes (i.e., *m***
939 **and *n* in Eq.1) are provided for the optimized algorithm.**

	Modes	NJU	PAES	NUIST	All the three sites	IMPROVE 2007	IMPROVE 1999
MSE of $(NH_4)_2SO_4$	small	2.32	2.02	2.43	2.29	2.2	-
	large	4.71	4.92	4.86	4.82	4.8	-
	overall	3.91	3.88	4.03	3.94	-	3
MSE for NH_4NO_3	small	2.67	2.48	2.56	2.62	2.4	-
	large	5.37	5.31	5.26	5.35	5.1	-
	overall	4.41	4.13	4.23	4.31	-	3
MSE of OM	small	4.4	4.56	4.22	4.46	2.8	-
	large	6.23	6.36	6.45	6.41	6.1	-
	overall	5.26	5.03	5.35	5.25	-	4
m	-	0.66	0.71	0.39	0.67	-	-
n	-	0.29	0.27	0.33	0.31	-	-
Sample number	-	174	45	63	282	-	-

940

https://doi.org/10.5194/acp-2020-176
Preprint. Discussion started: 28 April 2020

Atmospheric Chemistry and Physics Discussions

941 **Table 3. The source contributions of secondary aerosols to aerosol light**
942 **scattering at the three sites for the clean and polluted periods (%).**

Air quality level	Sources	NJU		PAES		NUIST	
		SIA	SOA	SIA	SOA	SIA	SOA
Clean	Coal combustion	6.6	0.8	6.5	1.1	7.5	1.3
	Industrial plants	5.8	3.6	4.2	1.5	8.2	6.3
	Vehicles	2.1	1.0	6.1	1.5	4.2	1.1
	Total	19.9		20.9		28.6	
Polluted	Coal combustion	12.4	1.6	8.8	2.3	10.2	2.2
	Industrial plants	10.2	5.8	7.8	3	12.6	9.9
	Vehicles	5.0	1.7	7.9	2.6	5.2	1.6
	Total	36.7		32.4		41.7	

943

https://doi.org/10.5194/acp-2020-176
Preprint. Discussion started: 28 April 2020

Atmospheric Chemistry and Physics Discussions

944 **Figure 1**

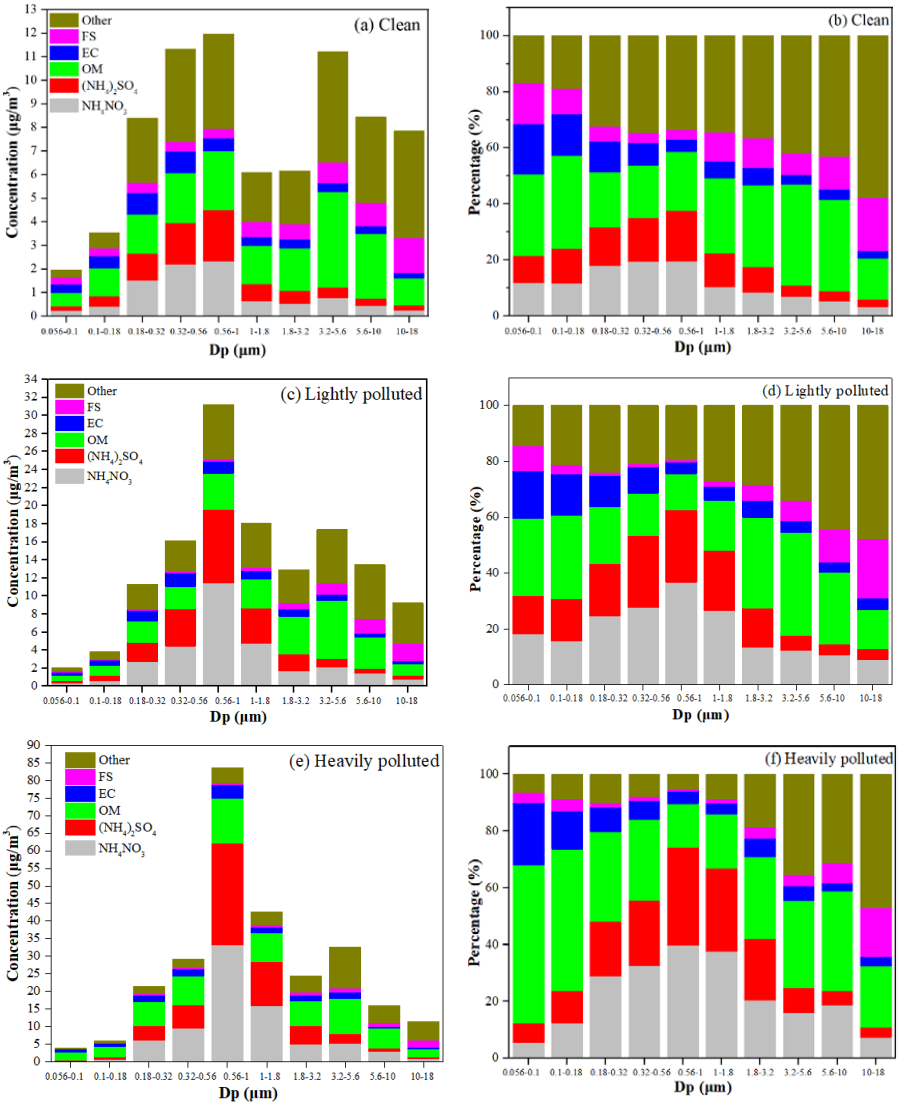

945

946

https://doi.org/10.5194/acp-2020-176
Preprint. Discussion started: 28 April 2020

Atmospheric Chemistry and Physics Discussions

947 **Figure 2**

948

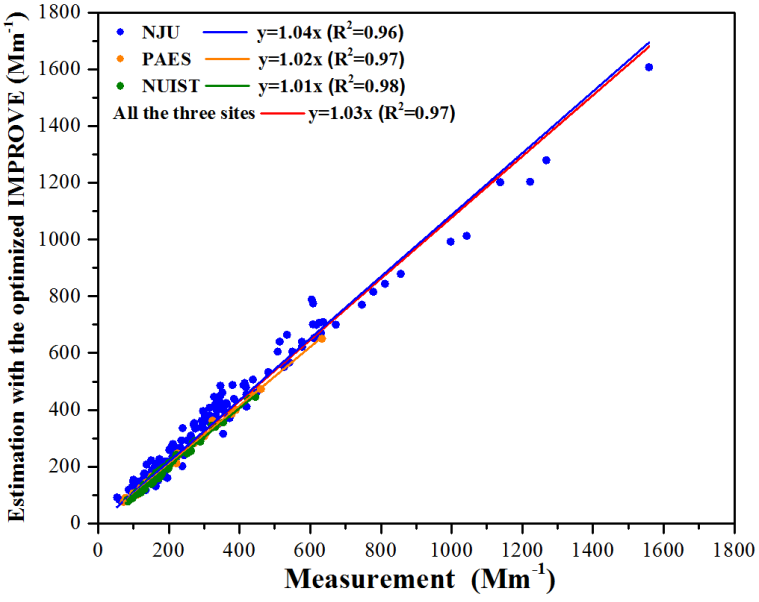

949

950

https://doi.org/10.5194/acp-2020-176
Preprint. Discussion started: 28 April 2020

Atmospheric Chemistry and Physics Discussions

951

952 **Figure 3**

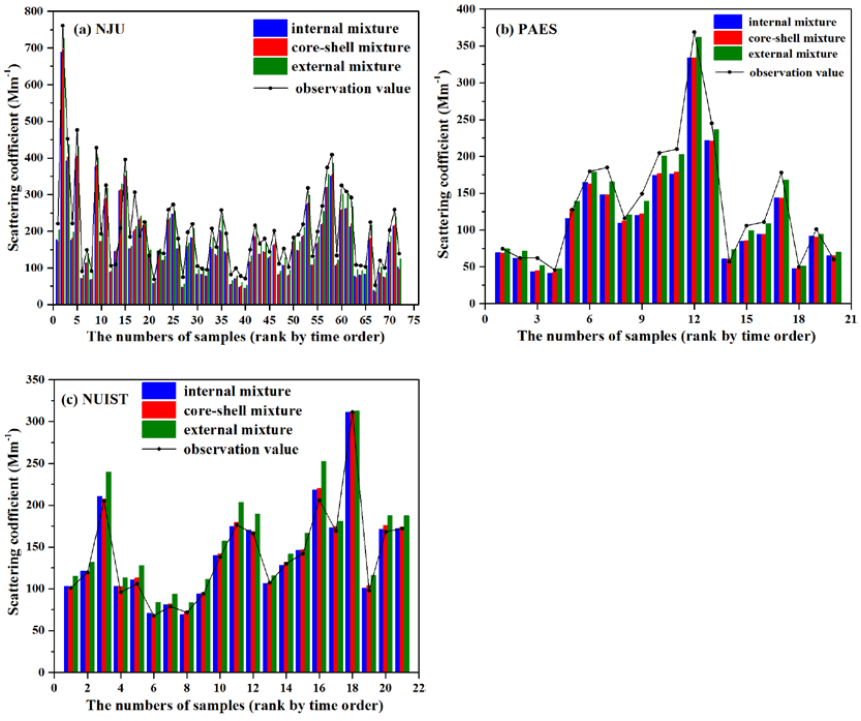

953

https://doi.org/10.5194/acp-2020-176
Preprint. Discussion started: 28 April 2020

Atmospheric Chemistry and Physics Discussions

954

955 **Figure 4**

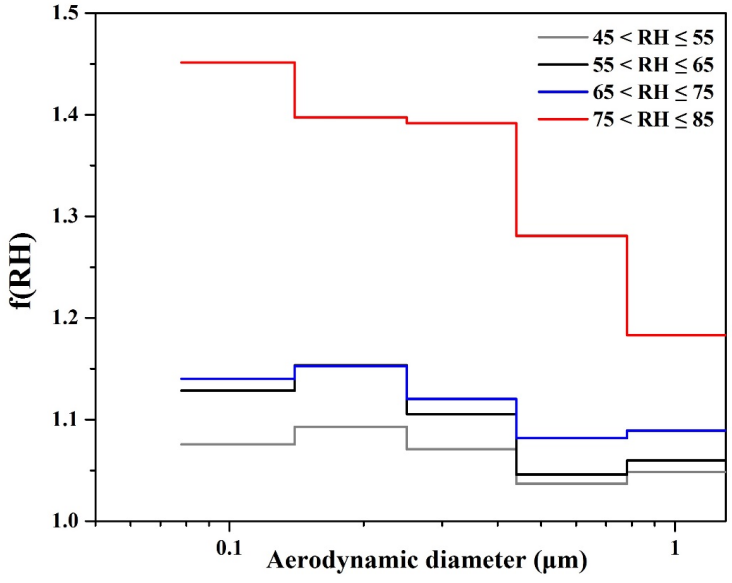

956

957

https://doi.org/10.5194/acp-2020-176
Preprint. Discussion started: 28 April 2020

Atmospheric Chemistry and Physics Discussions

958

959 **Figure 5**

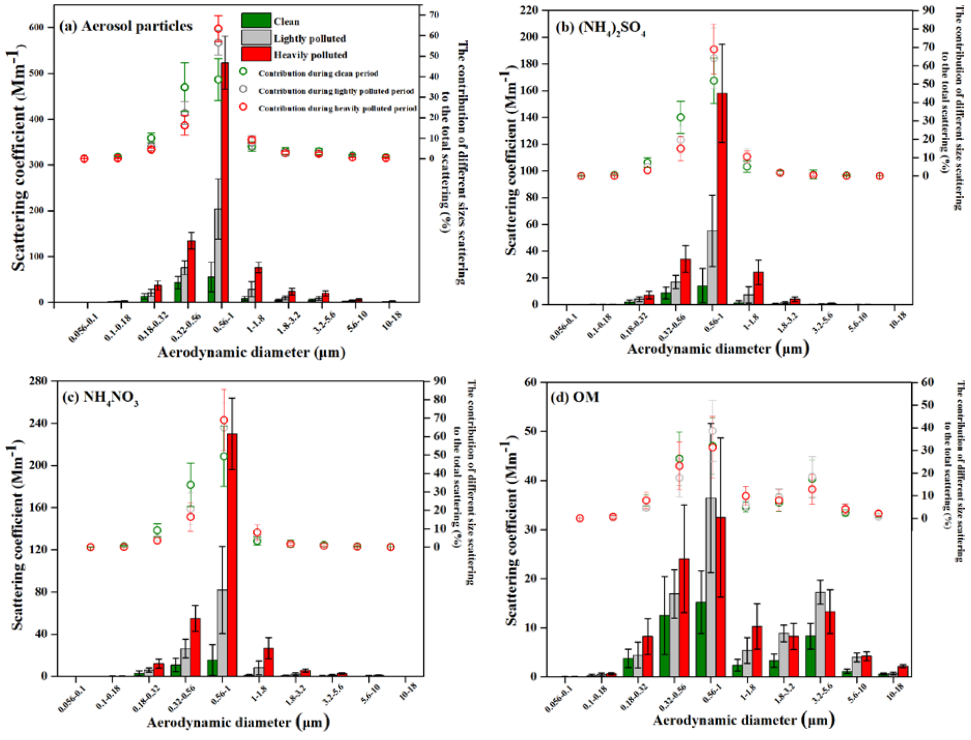

960

https://doi.org/10.5194/acp-2020-176
Preprint. Discussion started: 28 April 2020

Atmospheric Chemistry and Physics Discussions

961

962 **Figure 6**

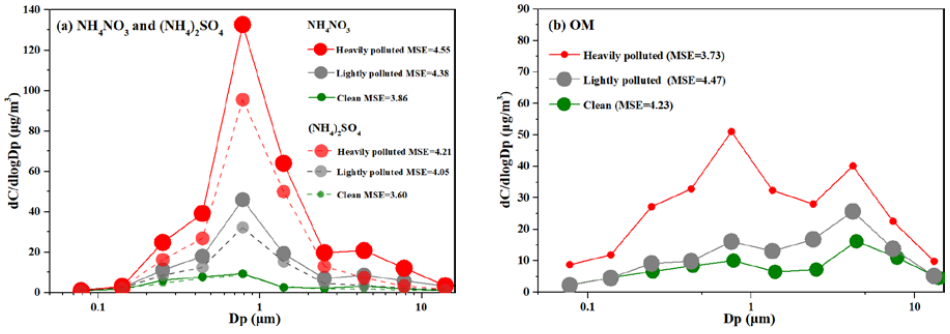

963

https://doi.org/10.5194/acp-2020-176
Preprint. Discussion started: 28 April 2020

964

965 **Figure 7**

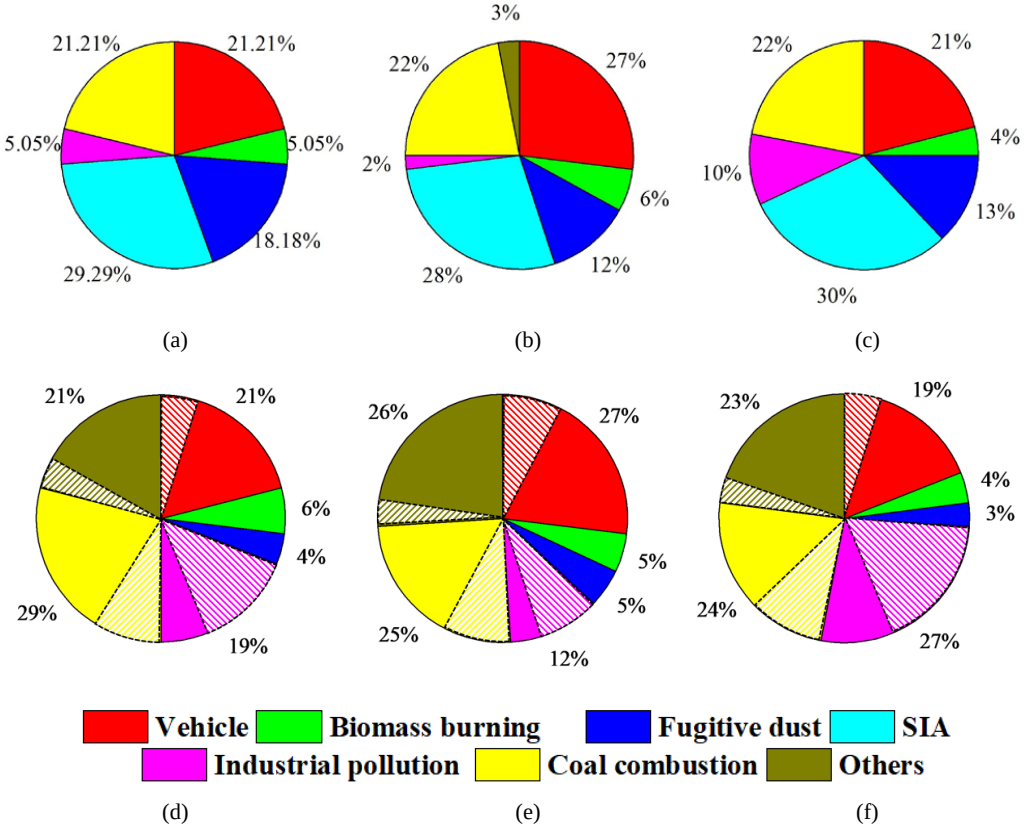

966

https://doi.org/10.5194/acp-2020-176
Preprint. Discussion started: 28 April 2020

967

968 **Figure 8**

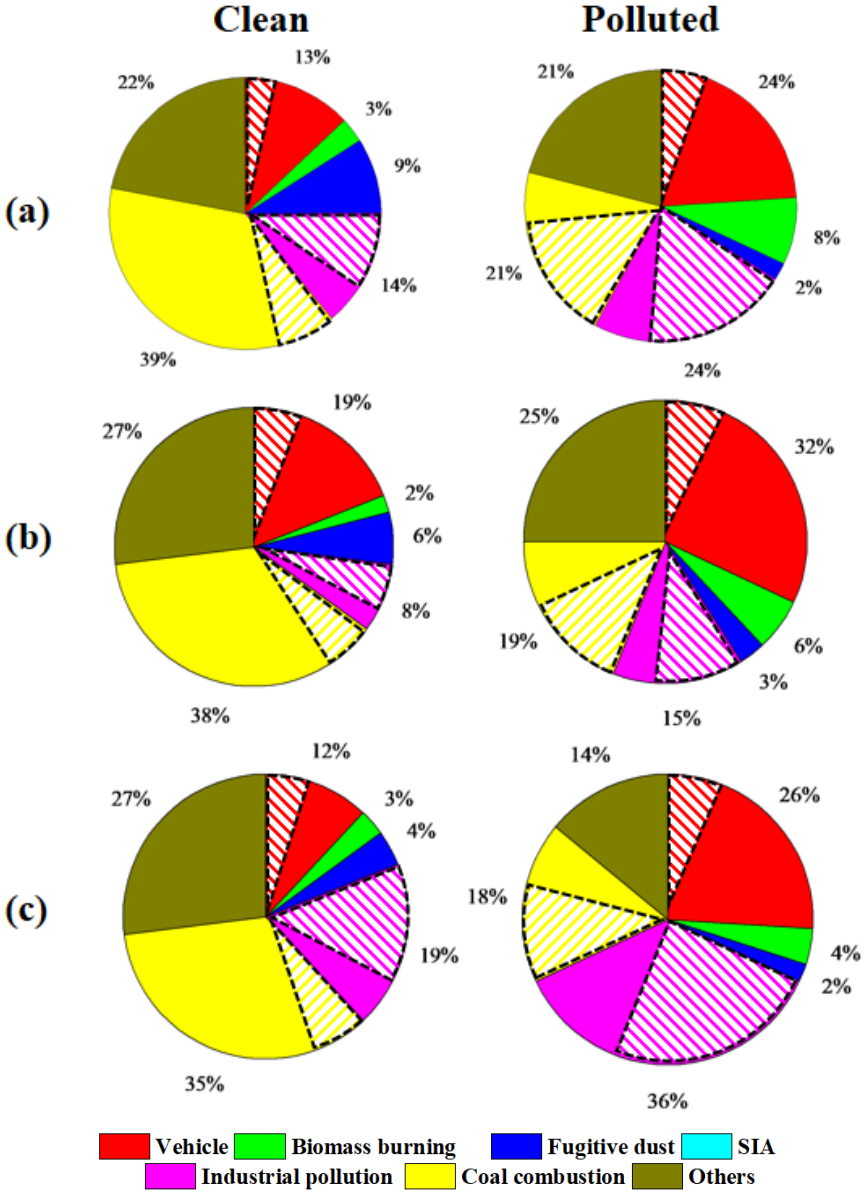

969

970